Electron attachment to a proton in water by interatomic Coulombic electron capture: An *R*-matrix study

Axel Molle [,1,2,*] Alain Dubois,[1] Jimena D. Gorfinkiel [,3] Lorenz S. Cederbaum [,4] and Nicolas Sisourat [1]

[1]*Sorbonne Université, CNRS, Laboratoire de Chimie Physique - Matière et Rayonnement, F-75005 Paris, France*
[2]*Quantum Chemistry and Physical Chemistry, Department of Chemistry, KU Leuven, Celestijnenlaan 200F, B-3001 Leuven, Belgium*
[3]*School of Physical Sciences, The Open University, Walton Hall, Milton Keynes MK7 6AA, United Kingdom*
[4]*Theoretische Chemie, Physikalisch-Chemisches Institut, Universität Heidelberg, Im Neuenheimer Feld 229, Heidelberg D-69120, Germany*

Interatomic Coulombic electron capture (ICEC) is an environment-enabled electron capture process in which a free electron can efficiently attach to a quantum system by transferring the excess energy to a neighbor thus ionizing it. Using the *ab initio R*-matrix method, we investigate the electron attachment to a proton in the neighborhood of a water molecule. The corresponding ICEC cross sections exhibit clear Fano profiles, resulting from interferences between the ICEC final states and resonant states. These Fano interferences, observed in the total ICEC cross sections, were discussed in our recent work on large system-neighbor separations [A. Molle *et al.*, Phys. Rev. A **103**, 012808 (2021)]. In the present study, we report on the ICEC cross sections at shorter distances which are relevant in biological and biochemical contexts. Furthermore, we investigate the partial ICEC cross sections and demonstrate that the ionization of a water molecule via ICEC is substantially different from that due to direct photoionization. Finally, we show that the distortion of the equilibrium geometry of the water molecule due to the presence of the proton influences the ICEC process.

I. INTRODUCTION

Interatomic Coulombic electron capture (ICEC) is an environment-enabled electron capture: it is a unique inelastic electron scattering process in which a free electron can efficiently attach to a quantum system [1–5] by transferring the released excess energy to a neighbor which is then ionized (see Fig. 1). This transfer can take place over large distances and has specific physical implications. For instance, it reduces one species (electron attachment) while oxidating another within the environment.

ICEC leads to a strong enhancement of the electron capture cross sections, which was theoretically demonstrated in several systems [1,2,6]. In a previous work, we have theoretically investigated the ICEC process with the *ab initio R*-matrix method in the example system of a proton in the neighborhood of a water molecule [7]. We have shown that the ICEC cross sections exhibit clear Fano profiles. The latter stem from the interferences between the ICEC final states and resonant states in which the incoming electron temporarily binds to the proton-water setup. Due to these interferences, the ICEC cross sections can be substantially enhanced or suppressed. In that previous study, we reported on the total cross sections at extremely large system-neighbor separations. In the present work, the ICEC cross sections at shorter distances are studied. In particular, we investigate whether the Fano profiles are sustained at these distances. Furthermore, the partial ICEC cross sections are reported and we demonstrate that the ionization

of a water molecule via ICEC is substantially different than by direct photoionization. Finally, the change of the water geometry due to the presence of the proton, compared to the isolated molecule, and the impact on ICEC are discussed.

II. METHODS AND COMPUTATIONAL DETAILS

The ICEC cross sections were computed with the *R*-matrix method as implemented in the UKRmol+ package. A review of the *R*-matrix method can be found in [8] and details of the UKRmol+ package are presented in [9]. In the following, we summarize the method and the implementation used in this study. In the *R*-matrix approach, the configuration space is partitioned into an inner and an outer region defined by a sphere of radius *a* around the center of mass of the proton-water system. The inner region contains the multielectron description of the full system composed of 11 electrons. In the outer region only a single electron is considered and its interaction with the 10 remaining electrons is described using a multipole expansion. The *R* matrix links the two regions. Analysis of the wave function (matching to asymptotic expressions) enables the determination of scattering-energy-dependent *K* matrices from which *T* matrices and therefore cross sections can be obtained, as well as other scattering quantities (see [9] and references therein).

We considered different geometries: in all of them a symmetric planar configuration where the oxygen atom points to the proton is assumed. The geometries differ by (i) the distance between the oxygen atom and the proton (noted *R* in the following) and (ii) the geometry of the water molecule. We consider ground state equilibrium geometry of the isolated

*nicolas.sisourat@upmc.fr

molecule and that of the molecule in the presence of the proton for different R. The geometries were computed at the MP2 level with the cc-pVDZ basis set using the MOLPRO package [10,11]. Note that the geometries employed in this work were not chosen to reproduce the properties of the proton-water system but to illustrate the fundamental ICEC mechanisms. Studies on the structures and properties of the proton-water system can be found in, e.g., [12].

As in our previous work [7], the R-matrix calculations are performed in the C_{2v} point group and within the fixed-nuclei approximation. We employed state-averaged complete active space self-consistent field (CASSCF) orbitals optimized for the three lowest singlet A_1 states: H^+-$H_2O(\tilde{X})$, H^+-$H_2O(\tilde{B})$, and $H(1s)$-$H_2O^+(3a_1^{-1})$. The active space includes the following orbitals: $1s_O$, $2s_O$, $1s_H$, $3a_1$, $4a_1$, $1b_1$, $1b_2$, and $2b_2$. In the R-matrix expansion, 18 target states (3 singlet and 3 triplet in each A_1, B_1, and B_2 symmetry), obtained from a full configuration interaction (CI) in the CAS active space, were included. They correspond to the 11 lowest states of H^+-H_2O and 7 lowest states of $H(1s)$-H_2O^+. The latter are the final states of the ICEC processes. The cc-pVDZ basis set was used and the CASSCF orbitals were optimized using the MOLPRO package [10,11]. We employed "continuum" orbitals with angular momentum up to $\ell = 6$, which are described with 25 B-spline type orbitals of order 6 in each ℓ. The R-matrix radius a was fixed at 25 a.u. and the maximum values in the Legendre expansion of the mixed nuclear attraction and 2-electron integrals were fixed at 35 and 45, respectively. For the outer region calculations, the R-matrix is propagated from a to 80 a.u.

The computed energies of the target states relevant for ICEC are reported and discussed in Appendix A. The additional energies of the excited states of H^+-H_2O are given and discussed in our previous work [7]. Note that at the considered electron energy range, ICEC leaving the water molecule in the deeper $(1b_2^{-1}, {}^2B_2)$ state is not energetically allowed. As shown in [7], this channel opens at incoming electron energies above about 4.0 eV. The equilibrium geometry of the water molecule computed for several distances to the proton is given in Appendix B.

III. RESULTS

A. Total ICEC cross sections as functions of *R*

We first discuss the total ICEC cross sections as functions of R. We investigate a range of R going from 3 Å to 8 Å. Note that in a Zundel-type configuration, the distance between the proton and the second solvation shell is between 3 and 4 Å [13]. The distances to the third shell lie in the upper part of the range considered in this work.

The cross sections computed with the R-matrix approach can be compared with those obtained with the virtual photon approximation. The latter is valid in the limit of large R and provides an analytical formula for the cross sections [1,2]:

$$\sigma_{\text{ICEC}}(\epsilon) = \frac{3\hbar^4 c^2}{8\pi m_e} \frac{g_H}{g_{H^+}} \frac{\sigma_{\text{PI}}^{(H)}(\epsilon)\sigma_{\text{PI}}^{(H_2O)}(\epsilon')}{\epsilon R^6 E_{\text{vph}}^2}, \quad (1)$$

where $\sigma_{\text{PI}}^{(H)}$ and $\sigma_{\text{PI}}^{(H_2O)}$ are the photoionization cross sections of atomic hydrogen and isolated water, respectively. The
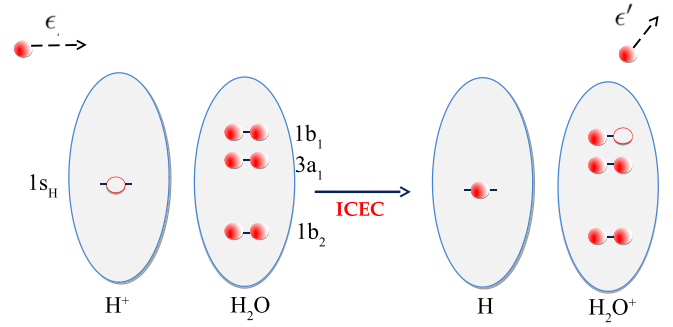
FIG. 1. ICEC scheme in the example system of a proton in the neighborhood of a water molecule: A free electron attaches to the proton. The attachment energy is transferred to the water molecule which is then ionized.

energies of the incoming and outgoing electrons are noted ϵ and ϵ'. The statistical weights of the quantum states are $g_H = 2$ and $g_{H^+} = 1$. The energy transferred between the species is $E_{\text{vph}} = \text{IP}_H + \epsilon$, where $\text{IP}_H = 13.61$ eV is the ionization potential of atomic hydrogen. In this work, we consider only ICEC processes for which the electron is captured in the ground state of hydrogen. The photoionization cross sections were taken from [14] and [15,16].

Figure 2 shows the total ICEC cross sections multiplied by R^6 for several R. The geometry of the water is that of the ground state equilibrium geometry of the isolated molecule. It is seen that above $R = 6$ Å except for the Fano profiles, the virtual photon approximation is valid. Below 6 Å the *ab initio* ICEC cross sections are much larger than predicted by the asymptotic formula. The large enhancement of the *ab initio* cross sections results from the contributions of the orbital overlaps between H and H_2O which are neglected in the derivation of the asymptotic formula (see [1,2] and [6]).

At large R, the ICEC cross sections exhibit clear Fano profiles, resulting from interferences between the ICEC final states and resonant states where the incoming electron is temporarily bound to the system. These Fano interferences were
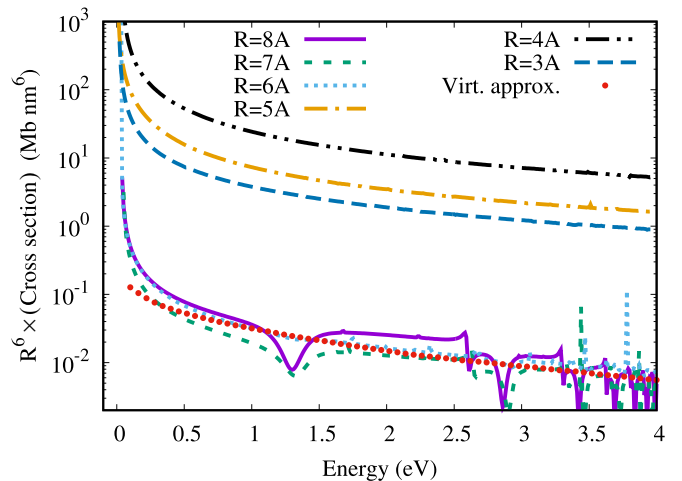
FIG. 2. Total ICEC cross sections multiplied by R^6: *ab initio* results compared with the asymptotic one of Eq. (1) (red dots).
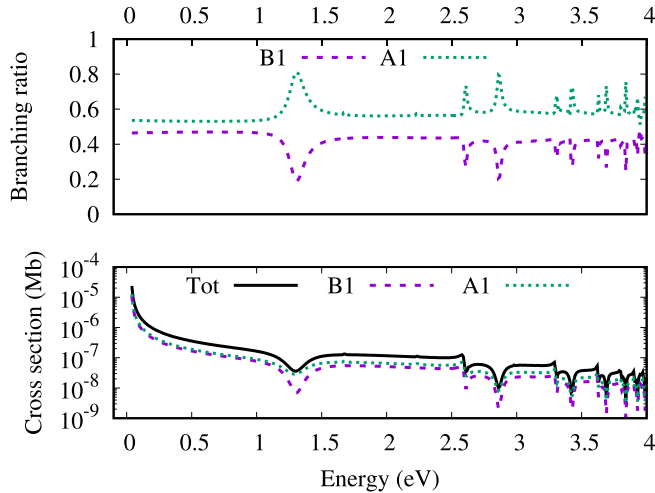
FIG. 3. Partial ICEC cross sections and branching ratio for $R = 8$ Å obtained with the R-matrix approach. The B_1 and A_1 branching ratios correspond to ICEC leaving the water molecule in the $(1b_1^{-1}, {}^2B_1)$ and $(3a_1^{-1}, {}^2A_1)$ states, respectively.

discussed in detail in our recent work [7]. Surprisingly, the Fano profiles disappear in the total ICEC cross sections at shorter R. Further insights are obtained by investigating the partial ICEC cross sections (i.e., ICEC channels leading to different electronic states of the ionized water molecule).

B. Partial ICEC cross sections as functions of R

The ICEC mechanism can lead to ionization of the water molecule in different cationic states. We present below the corresponding partial cross sections (σ_i^{ICEC}) and branching ratio. The latter is defined as

$$\text{BR}_i(\epsilon) = \frac{\sigma_i^{\text{ICEC}}(\epsilon)}{\sum_j \sigma_j^{\text{ICEC}}(\epsilon)}. \qquad (2)$$

In the partial cross sections, we have summed the singlet and triplet contribution for each ionized state i of the water molecule since both contributions do not differ significantly from each other.

Figures 3, 4, and 5 show the partial ICEC cross sections and branching ratio for $R = 8$, 6, and 4 Å, respectively. The B_1 and A_1 branching ratios correspond to ICEC leaving the water molecule in the $(1b_1^{-1}, {}^2B_1)$ and $(3a_1^{-1}, {}^2A_1)$ states, respectively. At $R = 8$ Å ionization of water leading to the $(3a_1^{-1}, {}^2A_1)$ state is slightly dominant. In the framework of the virtual photon approximation, the branching ratio can be obtained from the partial photoionization cross sections of isolated water. As shown in, for example, [17] photoionization leading to the $(3a_1^{-1}, {}^2A_1)$ water cation state is indeed dominant in the relevant photon energy range (i.e., $h\nu \approx$ 14–18 eV).

In general, the Fano interferences favor ionization to the $(3a_1^{-1}, {}^2A_1)$ state. Furthermore, at shorter distances, the presence of the proton greatly enhances the branching ratio of this state, reaching nearly 1 at $R = 4$ Å.

We now discuss the disappearance of the Fano profiles at shorter R. As seen in Fig. 5, Fano profiles are seen in the B_1 partial ICEC cross sections. However, these cross sections

are much smaller than those corresponding to the $(3a_1^{-1}, {}^2A_1)$ channel. It is therefore the couplings between the final ICEC $(3a_1^{-1}, {}^2A_1)$ state and the resonant states that become relatively weaker at shorter R compared to the direct ICEC contributions (see below). As a result, the Fano profiles play a less significant role. Since the energy of the resonances and the target states do not change significantly with the distance we think that the weaker couplings between the resonances and the $(3a_1^{-1}, {}^2A_1)$ state compared to that of the $(1b_1^{-1}, {}^2B_1)$ cation state comes from symmetry reason: the $1s$ orbital of hydrogen has an A_1 symmetry and can thus distort the $3a_1$ orbital of water. However, the $1s$ orbital of hydrogen does not overlap (or only weakly at the shortest R) with the $1b_1$ water orbital. Note that this symmetry reasoning might also explain the higher branching ratio for the A_1 states at shorter R.

We have calculated the branching ratio of the lowest A_1 resonance from the (normalized) eigenvectors associated with the largest eigenvalue of the time-delay matrix. Our calculations show that these rates depend only weakly on R which indicates that the couplings between the final ICEC $(3a_1^{-1}, {}^2A_1)$ state and the resonant states do not change significantly with R. These results therefore support our interpretation that it is the contribution of the direct ICEC path that becomes larger as R decreases compared to the ones involving resonances.

FIG. 4. Partial ICEC cross sections and branching ratio for $R = 6$ Å obtained with the R-matrix approach. The B_1 and A_1 branching ratios correspond to ICEC leaving the water molecule in the $(1b_1^{-1}, {}^2B_1)$ and $(3a_1^{-1}, {}^2A_1)$ states, respectively.
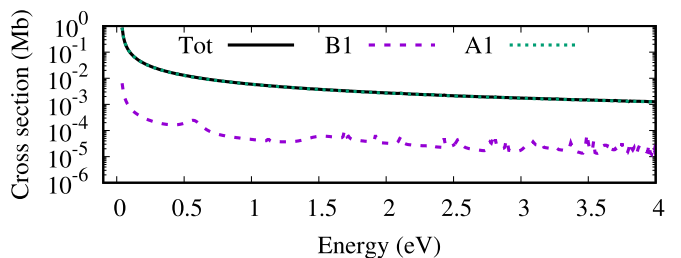
FIG. 5. Partial ICEC cross sections for $R = 4$ Å obtained with the R-matrix approach. The branching ratio for the $(3a_1^{-1}, {}^2A_1)$ state is nearly 1.
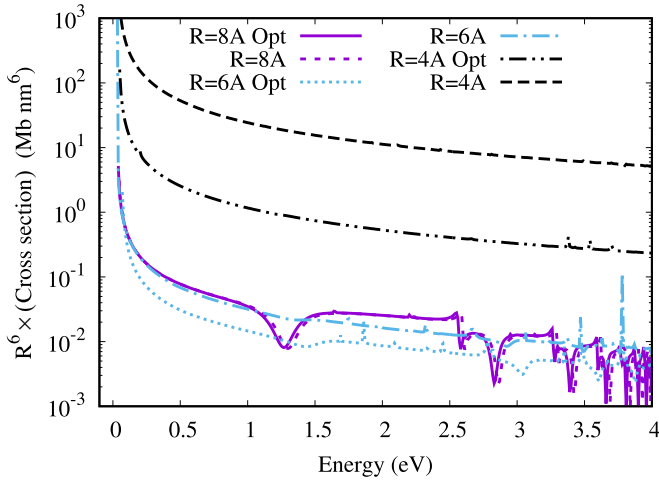
FIG. 6. Total *ab initio* ICEC cross sections at optimized geometries in the presence of a proton at R compared to those computed with the equilibrium geometry of the isolated water. The optimized geometries were obtained at the MP2 level with the cc-pVDZ basis set.

C. Equilibrium geometry of the water molecule in the presence of a proton at R

The results presented up until now (here and in our previous publication [7]) correspond to nonoptimized geometries. We have optimized the geometry of the molecule in the presence of H$^+$ for several R. In general, the presence of the proton does not influence the OH bond distances of the water molecule but leads to the opening of the HOH angle (the geometry parameters are listed in Appendix B). Figure 6 compares the total ICEC cross sections computed with the R-matrix approach for the two kinds of water molecule geometries. At the shorter R distances, the nuclear rearrangement lowers significantly the ICEC cross sections. As shown in the tables in Appendix A, the energies of the final states are lower at the optimized geometry of water in the presence of a proton at R with respect to the initial state. In general, the lower the energy transferred between the species the more efficient the ICEC process. The stabilization effects of the distorted geometries on the ICEC final states may therefore explain the decrease of the cross sections. We also mention that at the optimized geometries the charge distribution in the water molecule may be different than in the isolated equilibrium geometry which can also change the ICEC cross sections. However, these effects may lower or enhance the ICEC process.

IV. CONCLUSIONS

Following our previous work [7], we investigated the ICEC process in the system consisting of a proton in the neighborhood of a water molecule. The total and partial ICEC cross sections at proton-water distances between 3 and 8 Å are reported. This range corresponds to the second and third hydration shells in condensed phases and is thus relevant for biological and biochemical systems. We note that as protons are extremely reactive they do interact strongly with the first shell of water molecules which may influence the ICEC process between the proton and a molecule in a higher shell.

However, the investigation of larger systems exceeds the scope of the present work and has to be left for future studies.

Our results indicate that ICEC is an efficient process to neutralize a proton in a water environment. For example, the ICEC cross section [to H(1s)] at incoming energy of 1 eV and for distance between a proton and a water molecule of 4 Å is 100 times larger than the corresponding radiative capture cross section [18]. Furthermore, it is demonstrated that the ionization of the water molecule via ICEC favors ionization to the $(3a_1^{-1}, {}^2A_1)$ state compared to direct photoionization. Finally, we showed that the presence of the proton may distort the equilibrium geometry of the water molecule which eventually influences the ICEC process and the corresponding cross sections.

This work provides new insights into electron capture in water. In future studies, we will investigate less symmetrical arrangements as well as faster incoming electrons for which (i) deeper channels [e.g., $(1b_2^{-1}, {}^2B_2)$ state] open and (ii) the electron can be captured into a higher electronic state of hydrogen. Moreover, the current implementation of the R-matrix method will allow us to compute the ICEC cross sections for protons surrounded by more water molecules. Finally, it would be interesting to investigate how vibrational dynamics can influence the ICEC process. A full quantum description of vibrational and electronic dynamics for this kind of system is currently out of reach. Some approximate methods have been developed for electron-molecule scattering problems. However, ICEC involves two weakly bound species and can lead to large (shallow) vibrational motion. These approximate methods may therefore fail. Further theoretical works are needed in this direction.

TABLE I. Computed relative energies (in eV) of the target states included in the R-matrix calculations for $R = 3$, 4, and 8 Å and for the geometry of the isolated water.

R (Å)	Sym.	E (eV)	State
8	${}^1B_1$	0.0	H(1s)-H$_2$O$^+$($1b_1^{-1}$)
	${}^3B_1$	0.0	H(1s)-H$_2$O$^+$($1b_1^{-1}$)
	${}^1A_1$	2.29	H(1s)-H$_2$O$^+$($3a_1^{-1}$)
	${}^3A_1$	2.29	H(1s)-H$_2$O$^+$($3a_1^{-1}$)
	${}^1A_1$	2.50	H$^+$-H$_2$O($\tilde{X}$)
4	${}^1B_1$	0.0	H(1s)-H$_2$O$^+$($1b_1^{-1}$)
	${}^3B_1$	0.0	H(1s)-H$_2$O$^+$($1b_1^{-1}$)
	${}^1A_1$	2.15	H(1s)-H$_2$O$^+$($3a_1^{-1}$)
	${}^3A_1$	2.27	H(1s)-H$_2$O$^+$($3a_1^{-1}$)
	${}^1A_1$	2.33	H$^+$-H$_2$O($\tilde{X}$)
3	${}^1B_1$	0.0	H(1s)-H$_2$O$^+$($1b_1^{-1}$)
	${}^3B_1$	0.0	H(1s)-H$_2$O$^+$($1b_1^{-1}$)
	${}^1A_1$	1.53	H(1s)-H$_2$O$^+$($3a_1^{-1}$)
	${}^3A_1$	2.25	H(1s)-H$_2$O$^+$($3a_1^{-1}$)
	${}^1A_1$	2.62	H$^+$-H$_2$O($\tilde{X}$)

TABLE II. Computed relative energies (in eV) of the target states included in the R-matrix calculations for $R = 3$ and 4 Å for the optimized geometry of water in the presence of a proton.

R (Å)	Sym.	E (eV)	State
4	$^1B_1$	0.0	H(1s)-H$_2$O$^+(1b_1^{-1})$
	$^3B_1$	0.0	H(1s)-H$_2$O$^+(1b_1^{-1})$
	$^1A_1$	1.55	H(1s)-H$_2$O$^+(3a_1^{-1})$
	$^3A_1$	1.55	H(1s)-H$_2$O$^+(3a_1^{-1})$
	$^1A_1$	2.42	H$^+$-H$_2$O($\tilde{X}$)
3	$^1B_1$	0.0	H(1s)-H$_2$O$^+(1b_1^{-1})$
	$^3B_1$	0.0	H(1s)-H$_2$O$^+(1b_1^{-1})$
	$^1A_1$	1.15	H(1s)-H$_2$O$^+(3a_1^{-1})$
	$^3A_1$	1.42	H(1s)-H$_2$O$^+(3a_1^{-1})$
	$^1A_1$	2.45	H$^+$-H$_2$O($\tilde{X}$)

APPENDIX A

The computed energies of the relevant target states for several geometries are reported in Tables I and II. In all of the geometries a symmetric planar geometry where the oxygen atom points to the proton is assumed. Furthermore, we consider the ground state equilibrium geometry of the isolated molecule and that in the presence of the proton (computed at the MP2 level with the cc-pVDZ basis set). R is the distance between the oxygen atom and the proton. The initial ICEC state [H$^+$-H$_2$O(X)] is given in the bottom row of each section, and the final ICEC states [H(1s)-H$_2$O$^+$] in the other rows.

TABLE III. Equilibrium geometry of the water molecule computed for several distances to the proton R. The geometries were obtained at the MP2 level with the cc-pVDZ basis set. At $R > 4$ Å, the geometries do not change significantly compared to the asymptotic one ($R = \infty$).

R (Å)	OH bond distance (Å)	HOH angle (deg)
3	0.98	119.6
4	0.97	116.7
∞	0.97	101.6

As shown in the tables, the singlet and triplet states in each symmetry of the water cation are nearly degenerate in energy except at the shortest distance ($R = 3$ Å). The energies of the target states obtained at the two kinds of geometry (i.e., of the isolated molecule and of the distorted ones due to the presence of the proton) differ at short R (3 and 4 Å). As discussed in the main text, these differences impact significantly the ICEC process and its cross sections. Note that for larger R (>4 Å), the energies computed at the two geometries do not change significantly (not shown).

APPENDIX B

The equilibrium geometry of the water molecule computed for several distances to the proton are given in Table III. As shown in the table, the presence of the proton does not change significantly the OH bond distance compared to the isolated water molecule. However, as the proton approaches the water molecule the HOH angle opens.

[1] K. Gokhberg and L. S. Cederbaum, J. Phys. B **42**, 231001 (2009).

[2] K. Gokhberg and L. S. Cederbaum, Phys. Rev. A **82**, 052707 (2010).

[3] A. Bande, K. Gokhberg, and L. S. Cederbaum, J. Chem. Phys. **135**, 144112 (2011).

[4] F. M. Pont, A. Bande, and L. S. Cederbaum, Phys. Rev. B **88**, 241304(R) (2013).

[5] A. Molle, E. R. Berikaa, F. M. Pont, and A. Bande, J. Chem. Phys. **150**, 224105 (2019).

[6] N. Sisourat, T. Miteva, J. D. Gorfinkiel, K. Gokhberg, and L. S. Cederbaum, Phys. Rev. A **98**, 020701(R) (2018).

[7] A. Molle, A. Dubois, J. D. Gorfinkiel, L. S. Cederbaum, and N. Sisourat, Phys. Rev. A **103**, 012808 (2021).

[8] J. Tennyson, Phys. Rep. **491**, 29 (2010).

[9] Z. Mašín, J. Benda, J. D. Gorfinkiel, A. G. Harvey, and J. Tennyson, Comput. Phys. Commun. **249**, 107092 (2020).

[10] H.-J. Werner, P. J. Knowles, G. Knizia, F. R. Manby, and M. Schütz, WIREs Comput. Mol. Sci. **2**, 242 (2012).

[11] H.-J. Werner, P. J. Knowles, G. Knizia, F. R. Manby, M. Schütz, P. Celani, W. Györffy, D. Kats, T. Korona, R. Lindh, A. Mitrushenkov, G. Rauhut, K. R. Shamasundar, T. B. Adler, R. D. Amos, A. Bernhardsson, A. Berning, D. L. Cooper, M. J. O. Deegan, A. J. Dobbyn *et al.*, Molpro, version 2015.1, a package of *ab initio* programs, 2015, https://www.molpro.net.

[12] X. Huang, S. Carter, and J. M. Bowman, J. Phys. Chem. B **106**, 8182 (2002).

[13] F. Mouhat, Fully quantum dynamics of protonated water clusters, Condensed Matter [cond-mat], Sorbonne Université, 2018.

[14] W. Cunto, C. Mendoza, F. Ochsenbein, and C. J. Zeippen, Bulletin d'Information du Centre de Donnees Stellaires, Astron. Astrophys. **275**, L5 (1993).

[15] Leiden Database for Photodissociation and Photoionization of Astrophysically Relevant Molecules, https://home.strw.leidenuniv.nl/~ewine/photo/cross_sections.html.

[16] A. N. Heays, A. D. Bosman, and E. F. van Dishoeck, Astron. Astrophys. **602**, A105 (2017).

[17] A. J. Blake and J. H. Carver, J. Chem. Phys. **47**, 1038 (1967).

[18] M. Pajek and R. Schuch, Phys. Rev. A **45**, 7894 (1992).